



---

## Figures and figure supplements

Distinct myocardial lineages break atrial symmetry during cardiogenesis in zebrafish

**Almary Guerra et al**

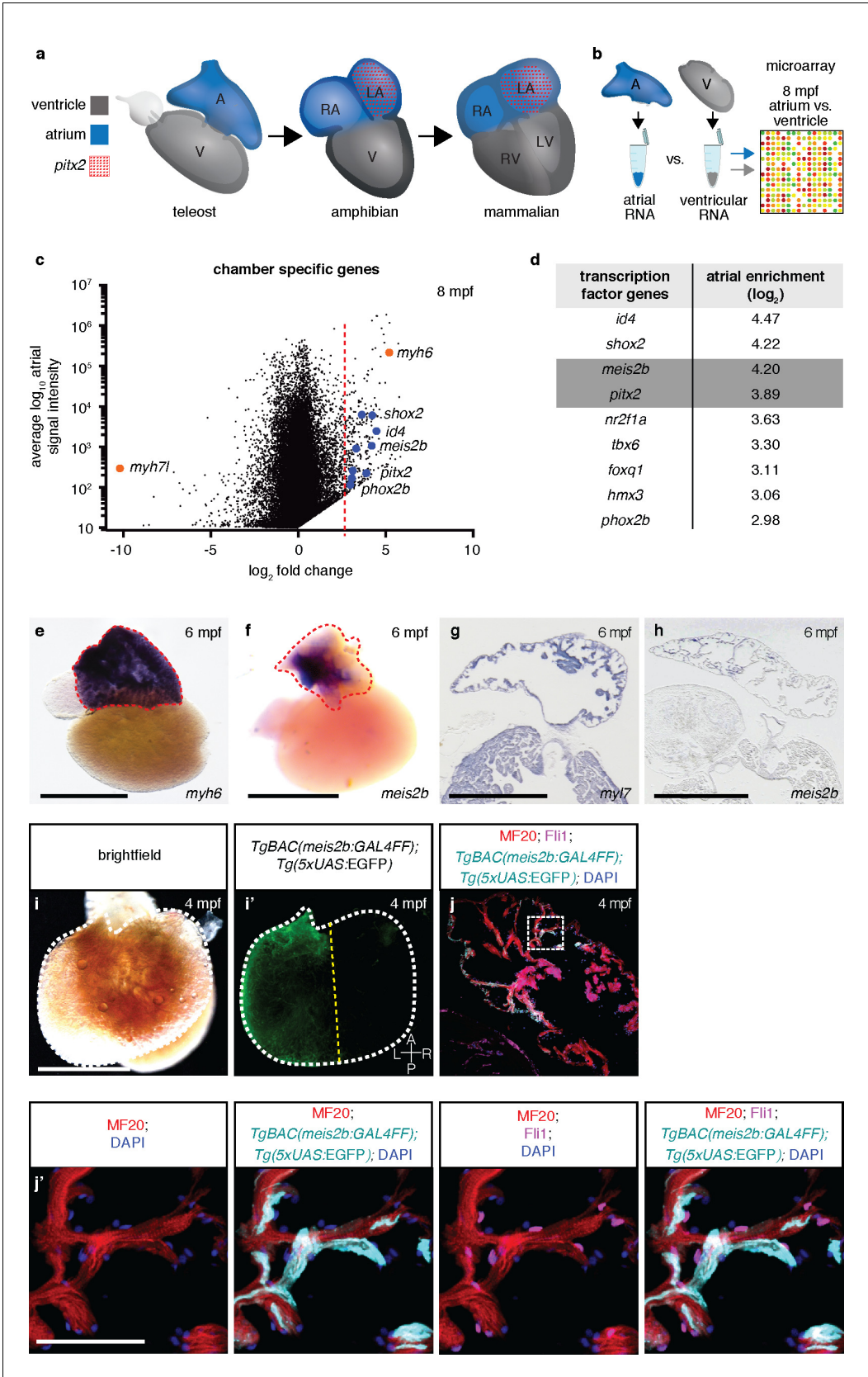
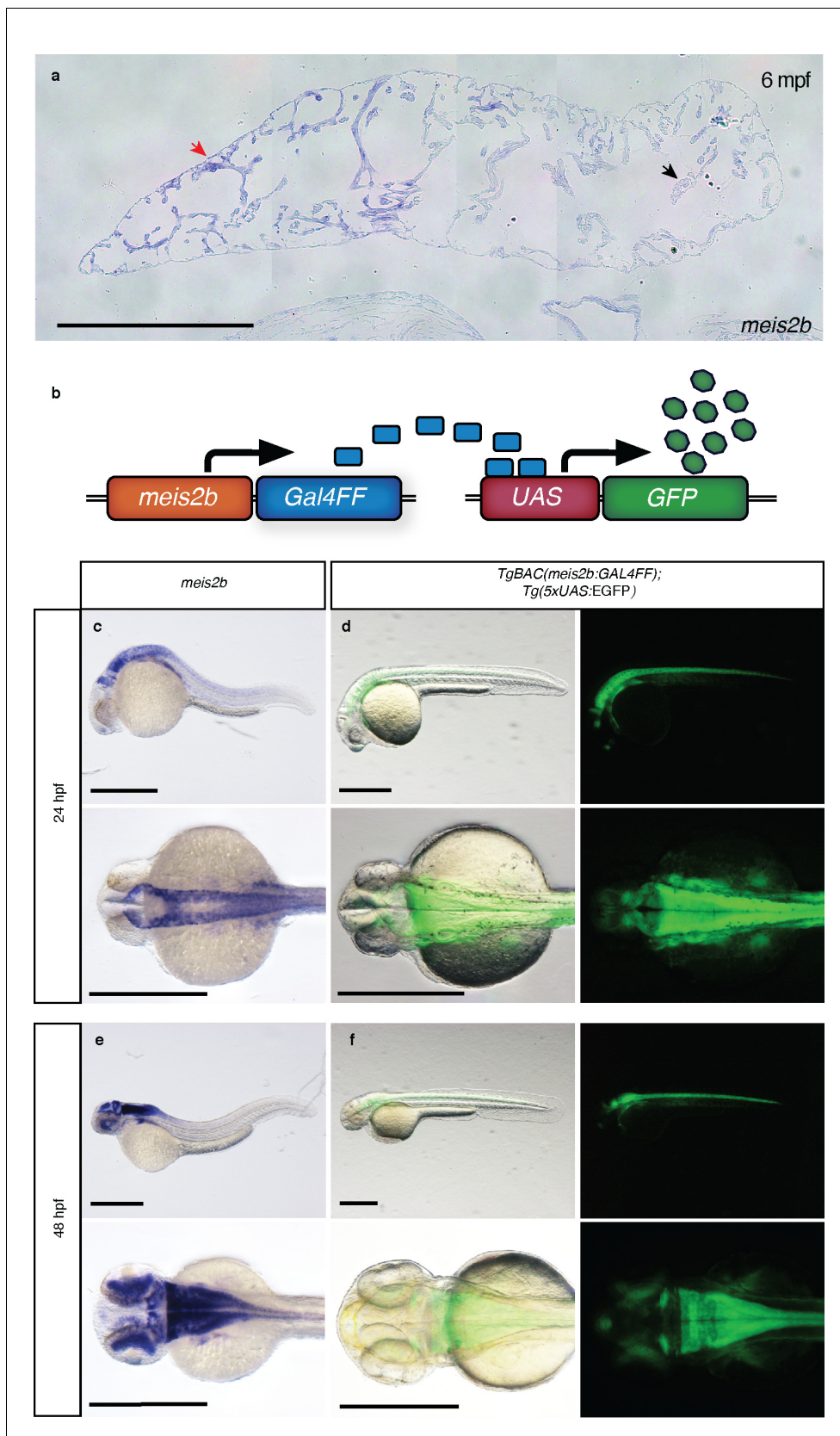


**Figure 1.** Asymmetric expression of atrial-specific transcription factor genes in adult zebrafish. (a) Comparison of different vertebrate hearts showing the emergence of distinct left and right chamber identities and atrial Figure 1 continued on next page

## Figure 1 continued

septation. (b) Schematic representation of the workflow for the identification of cardiac chamber-specific transcription factor gene expression. (c) Atrial gene expression level (signal intensity) and chamber-specific enrichment in the atrium (fold change >0) or ventricle (fold change <0). Red line marks 2.5 ( $\log_2$ ) fold cutoff. Highly enriched atrial transcription factor genes (blue), ventricular (*myh7l*) and atrial (*myh6*) chamber-specific myosin genes (orange) are shown. (d) Atrial enriched transcription factor genes ( $\log_2$  fold change >2.5). (e–f) Whole-mount in situ hybridization on adult zebrafish hearts; *myh6* expression covers the entire atrium while *meis2b* expression is restricted to the left side of the atrium. (g–h) In situ hybridization on adult cardiac sections; *myl7* is expressed in all cardiomyocytes while *meis2b* is expressed on the left side of the atrium in the wall and trabeculae (see **Figure 1—figure Supplement 1a** for higher magnification). (i–i') Brightfield and fluorescence images of a 4 mpf *Tg(meis2b-reporter)* zebrafish atrium. (j–j') High-magnification confocal projections of a 4 mpf *Tg(meis2b-reporter)* heart showing expression of the *Tg(meis2b-reporter)* in the myocardium (*Tg(meis2b-reporter)*+/*MF20*+/*Fli1* cells) but not the endocardium (*Tg(meis2b-reporter)*-/*MF20*-/*Fli1*+cells). (e–f, i–i') Red and white dotted lines delineate the atrium; (i') yellow line delineates *Tg(meis2b-reporter)* expression. Scale bars: (e–i) 1 mm, (j') 50  $\mu$ m.

DOI: <https://doi.org/10.7554/eLife.32833.002>



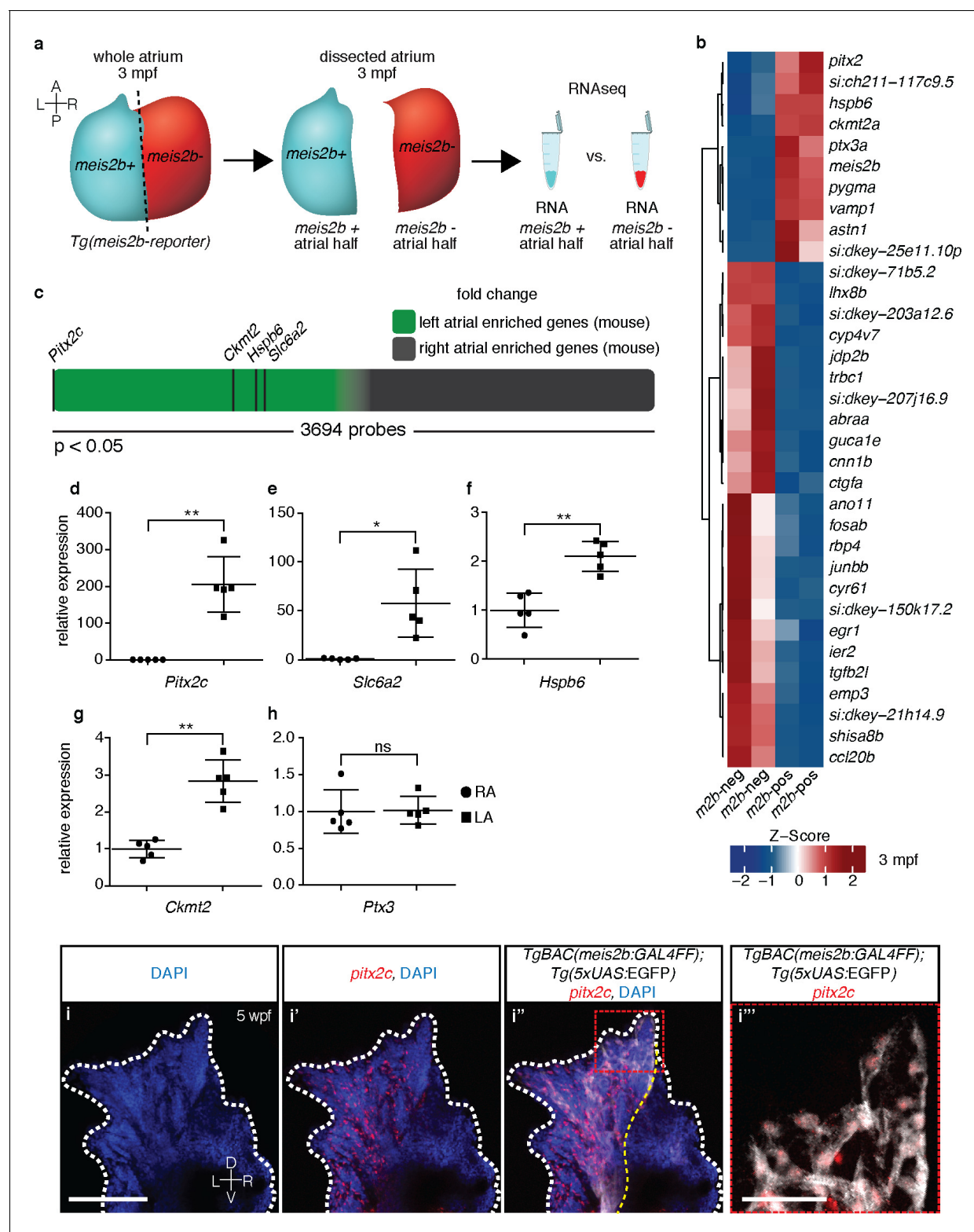
**Figure 1—figure supplement 1.** Validation of the *meis2b* reporter line. (a) High magnification of **Figure 1g** showing the asymmetric expression of *meis2b* in the atrium of the adult zebrafish heart (red arrow, *meis2b* + atrial domain; black arrow, *meis2b*- atrial domain). (b) Schematic of the *TgBAC* **Figure 1—figure supplement 1 continued on next page**



Figure 1—figure supplement 1 continued

(*meis2b*:GAL4FF);*Tg*(5xUAS:EGFP) *meis2b* reporter system. (c–f) Comparison of *meis2b* expression as detected by whole-mount in situ hybridization and *Tg*(*meis2b*-reporter) expression at 24 and 48 hpf. Note: in situ hybridization staining reaction was stopped before spinal CNS expression was fully detected in order to avoid overstaining of the head region. Scale bars: 500  $\mu$ m.

DOI: <https://doi.org/10.7554/eLife.32833.003>



**Figure 2.** The zebrafish atrium is divided into two transcriptionally distinct domains. (a) Schematic illustrating the dissection of a *Tg(meis2b-reporter)* atrium into *Tg(meis2b-reporter)*-positive and -negative domains for RNAseq analysis. (b) Global heatmap depicting Z-score of differentially expressed genes between *Tg(meis2b-reporter)*-positive and -negative domains (*m2b-pos* and *m2b-neg*, respectively). Red color indicates higher expression and blue color lower expression in the respective sample listed at the bottom of each column. (c) Schematic representation of asymmetrically expressed transcripts in mouse atria as determined by microarray analysis (Kahr et al., 2011); only significantly differentially expressed genes included (3695/ Figure 2 continued on next page

## Figure 2 continued

25697 probes). Green: significantly left atrial enriched transcripts; grey: significantly right atrial enriched transcripts. (d–h) RT-qPCR analysis of left vs. right atria in adult mouse shows that the orthologues of the most significantly enriched genes in the *Tg(meis2b-reporter)*-positive domain are also significantly enriched in the left atrium in mouse. Plots show relative gene expression in left atrium with respect to right atrium (n = 5). (i–i''') Wholemount fluorescent in situ hybridization (RNAscope) for *pitx2c* expression on a *Tg(meis2b-reporter)* zebrafish atrium [DAPI in blue, *Tg(meis2b-reporter)* in white, *pitx2c* in red]. (b–c, e) *si:ch211-117c9.5* is a zebrafish orthologue of *Slc6a2*. (i–i'') Red and white dotted lines delineate the atrium; (i') yellow line delineates *Tg(meis2b-reporter)* expression. (d–h) Two-tailed student t-tests were performed, \*p<0.05; \*\*p<0.005; \*\*\*p<0.0005; error bars indicate  $\pm$ SD. Scale bars: (i) 100  $\mu$ m, (i''') 25  $\mu$ m.

DOI: <https://doi.org/10.7554/eLife.32833.004>

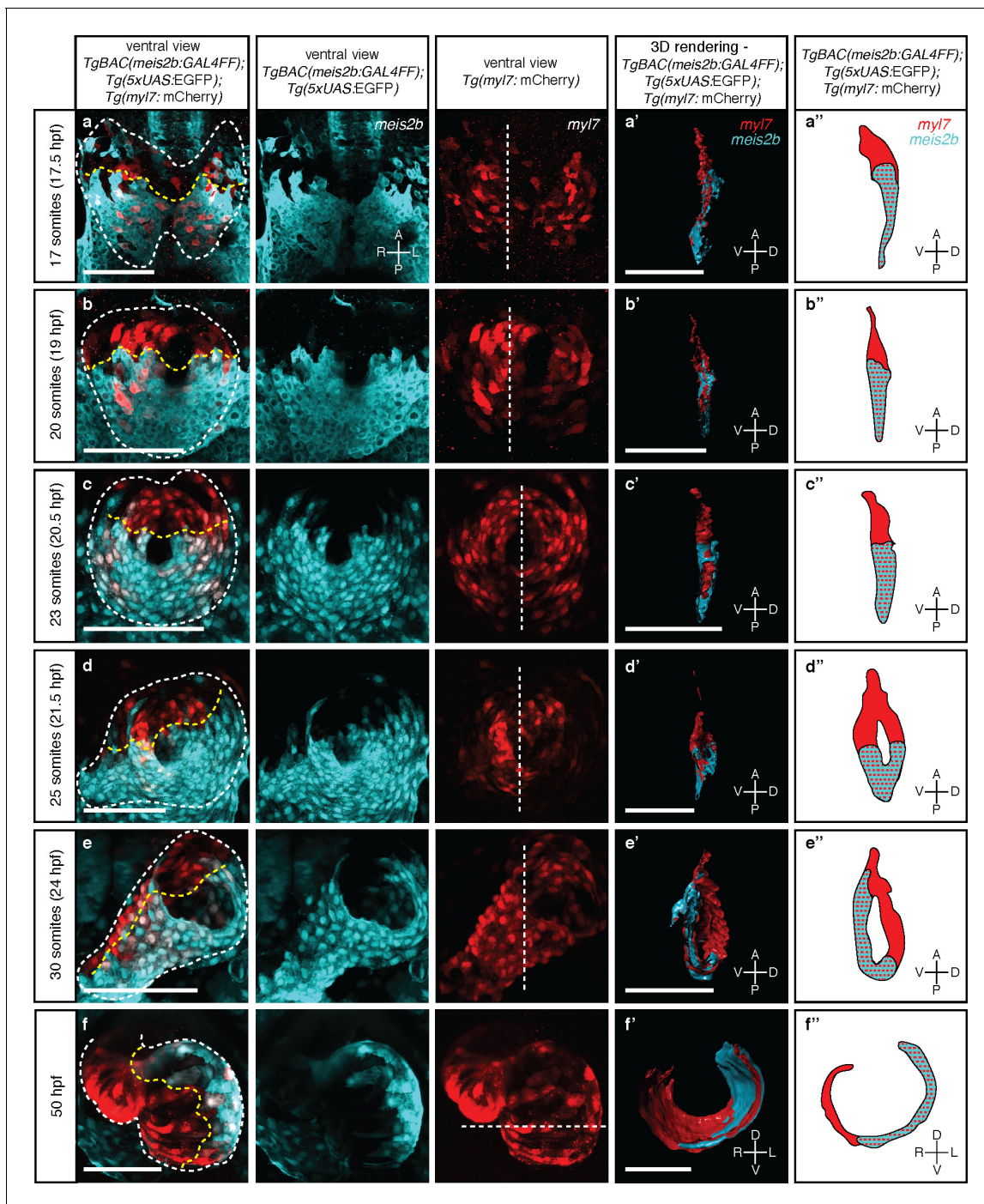


**Figure 3.** Myocardial morphogenesis establishes left-right laterality from two distinct antero-posterior fields. Confocal projections of *Tg(meis2b-reporter);Tg(myf7:mCherry)* embryos between the 17 ss (16 hpf) and 50 hpf. (a-c) Myocardial progenitors migrate to the midline and form the cardiac disc, where *Tg(meis2b-reporter)* expression is confined to the posterior compartment of the cardiac disc (PDC). (d) Cardiomyocytes forming the cardiac disc appear to migrate clock-wise, rotating the forming heart tube. (e) *Tg(meis2b-reporter)*-expressing cells are located on the ventral side of the heart tube. (f) At 50 hpf, *Tg(meis2b-reporter)* expression appears on the left side of the atrium, and in a small part of the ventricle near the AV canal. (a'-f') 3D rendered sections (as indicated in the third column, white dotted lines) of the hearts shown in a-f (see **Figure 3—videos 1–6** for full reconstructions). (a''-f'') Schematic representation of *Tg(meis2b-reporter);Tg(myf7:mCherry)* expression from (a'-f'). White dotted lines delineate the heart, yellow dotted lines delineate *Tg(meis2b-reporter)* expression. White dotted lines in third column indicate the level of the sagittal and transverse views. First to third columns: ventral views, anterior up; (a'-e', a''-e'') sagittal views, anterior up; (f', f'') transverse views, dorsal up. Scale bars: (a-e') 100 μm, (f') 50 μm.

DOI: <https://doi.org/10.7554/eLife.32833.006>

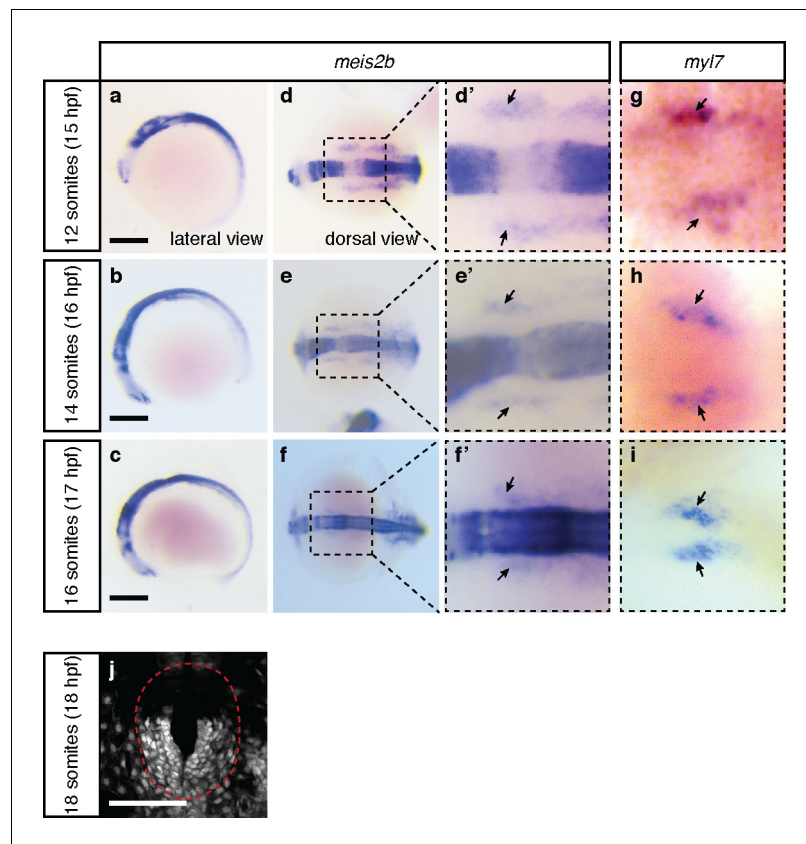


**Figure 3—figure supplement 1.** *meis2b* is expressed in the cardiogenic anterior lateral plate mesoderm. Whole-mount in situ hybridization for *meis2b* (a–f) and *myl7* (g–i) expression at several embryonic stages. Arrows point to expression of *meis2b* (d'–f') and the cardiomyocyte marker *myl7* (g–i) in the same region of the ALPM. (j) Confocal projection of *Tg(meis2b-reporter)* expression at 18 ss. (a–c) Lateral views, anterior to the left; (d–i) Dorsal views, anterior to the left; (j) red dotted line delineates the cardiac disc. Scale bars: 100  $\mu$ m.

DOI: <https://doi.org/10.7554/eLife.32833.007>



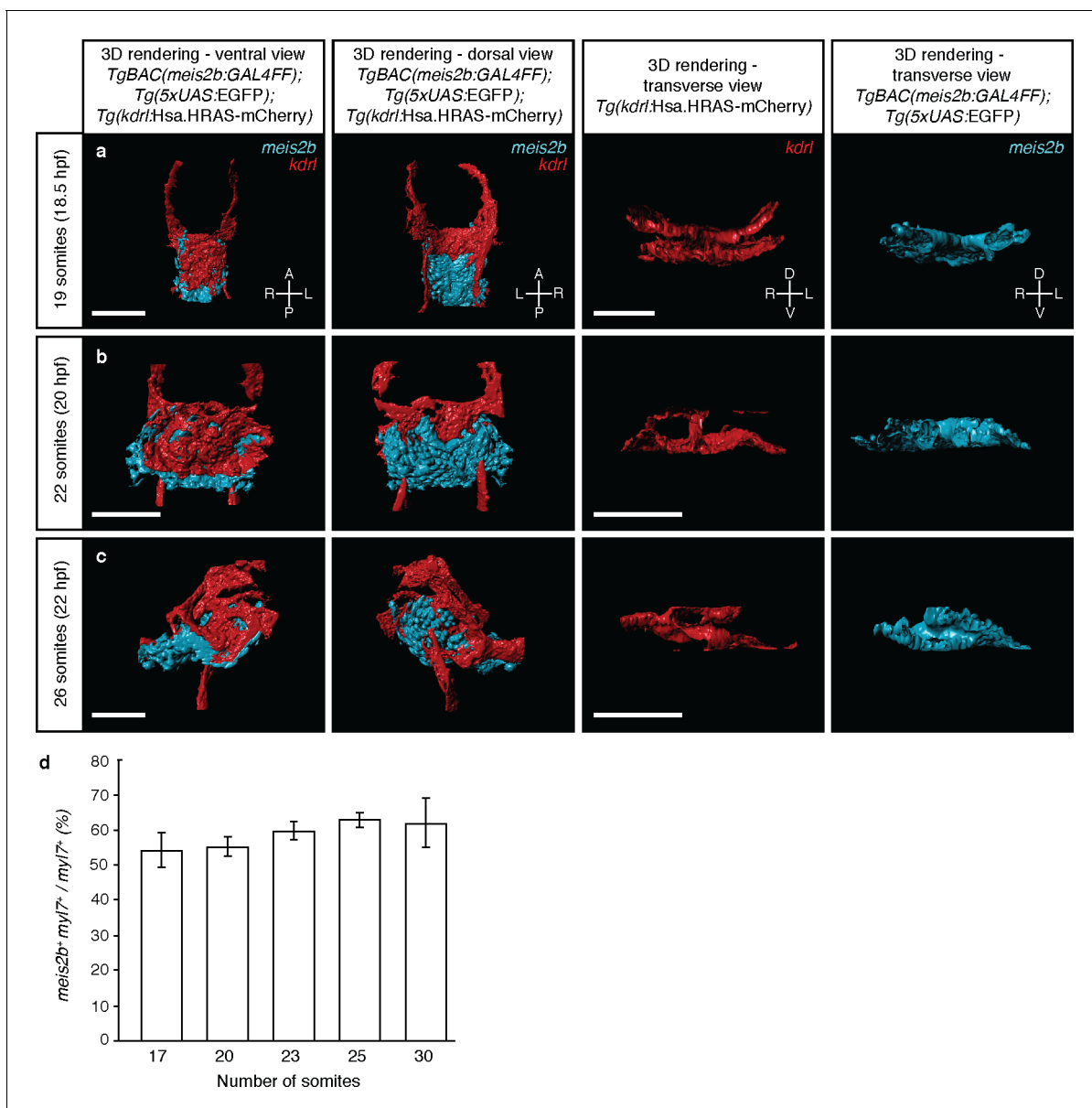
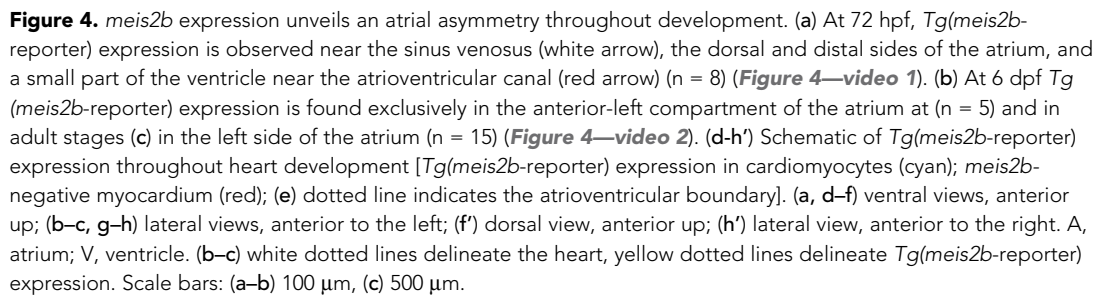


**Figure 3—figure supplement 2.** *Tg(meis2b-reporter)* expression with respect to the endothelium during the cardiac disc and heart tube stages. 3D surface rendering of *Tg(meis2b-reporter);Tg(kdrl:Hsa.HRAS-mCherry)* embryos at 19 to 26 ss. (a) At 19 ss, endocardial cells are located ventral to the myocardium and pass through the ring of myocardial cells to connect dorsally to the aortic arches. (b) At 22 ss, endocardial cells cover most of the ventral side of the myocardium in the cardiac disc. (c) At 26 ss, *Tg(meis2b-reporter)* expression is observed in the ventral side of the heart tube, while endocardial cells are lining the interior of the heart tube. Left column: ventral views, anterior up. Second column: dorsal views, anterior up. Third and fourth column: transverse views, dorsal up. (d) Percentage of *Tg(meis2b-reporter)*-positive cardiomyocytes with respect to the total number of *myl7*<sup>+</sup> cardiomyocytes from 17 to 30 ss. Scale bars: 100  $\mu$ m.

DOI: <https://doi.org/10.7554/eLife.32833.008>



Guerra et al. eLife 2018;7:e32833. DOI: <https://doi.org/10.7554/eLife.32833>

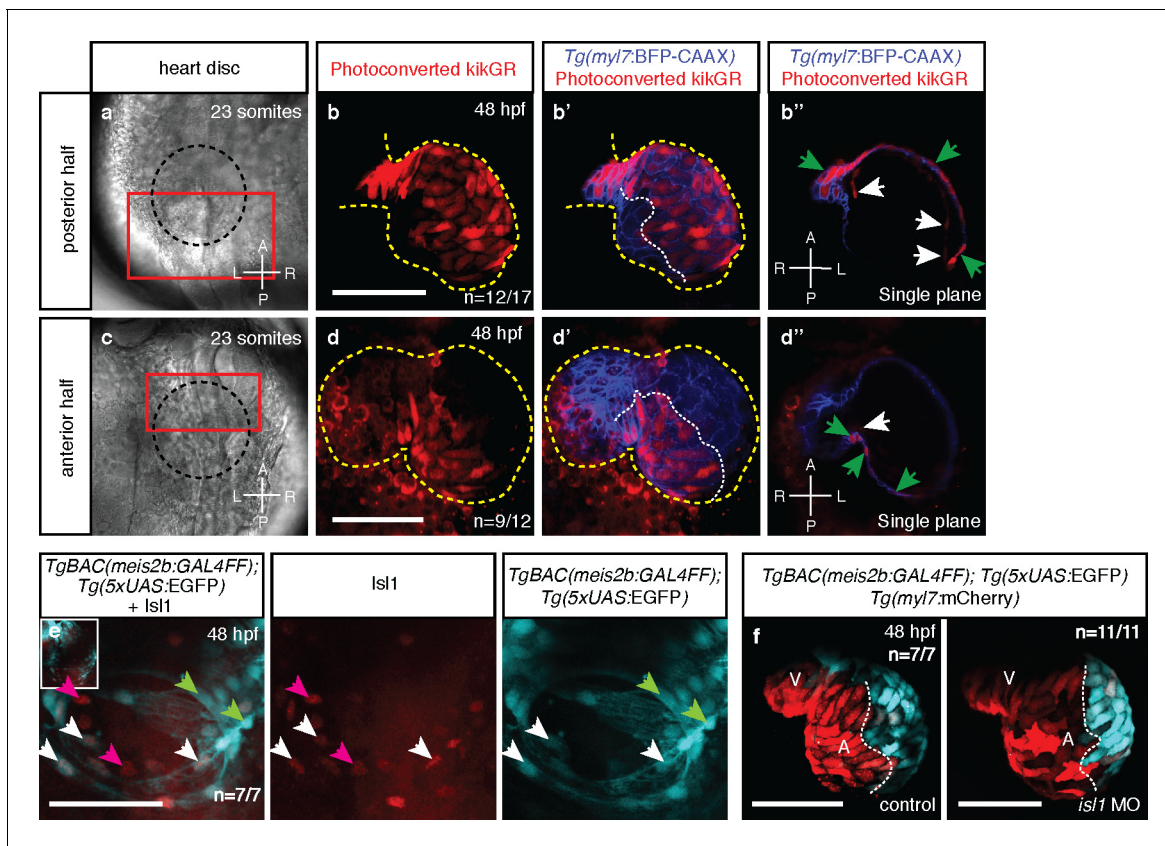


**Figure 5.** Atrial laterality is established from distinct antero-posterior fields without contribution from the second heart field. (a, c) Cardiac disc (dotted circle) at 23 ss. (b–b') Confocal projections of photoconverted kikGR with *Tg(myl7:BFP-CAAX)* hearts (yellow lines) show that cells from the PDC populate the left side of the atrium while (d–d') cells from the ADC populate the right side of the atrium (white dotted lines). (b'', d'') Single optical planes from b' and d', respectively (cardiomyocytes, green arrows; endocardial cells, white arrows). (e) *Tg(meis2b-reporter)* expression and antibody staining for *Isl1* in the 48 hpf heart [*meis2b*+/*Isl1*+ (white arrows), *meis2b*+/*Isl1*- (green arrows) and *meis2b*-/*Isl1*+ (pink arrows) cardiomyocytes]. (f) Confocal projections of control uninjected and *isl1* MO injected 48 hpf *Tg(meis2b-reporter)*; *Tg(myl7:mCherry)* hearts [white lines delineate *Tg(meis2b-reporter)* expression]. Scale bars: 100  $\mu$ m.

DOI: <https://doi.org/10.7554/eLife.32833.019>

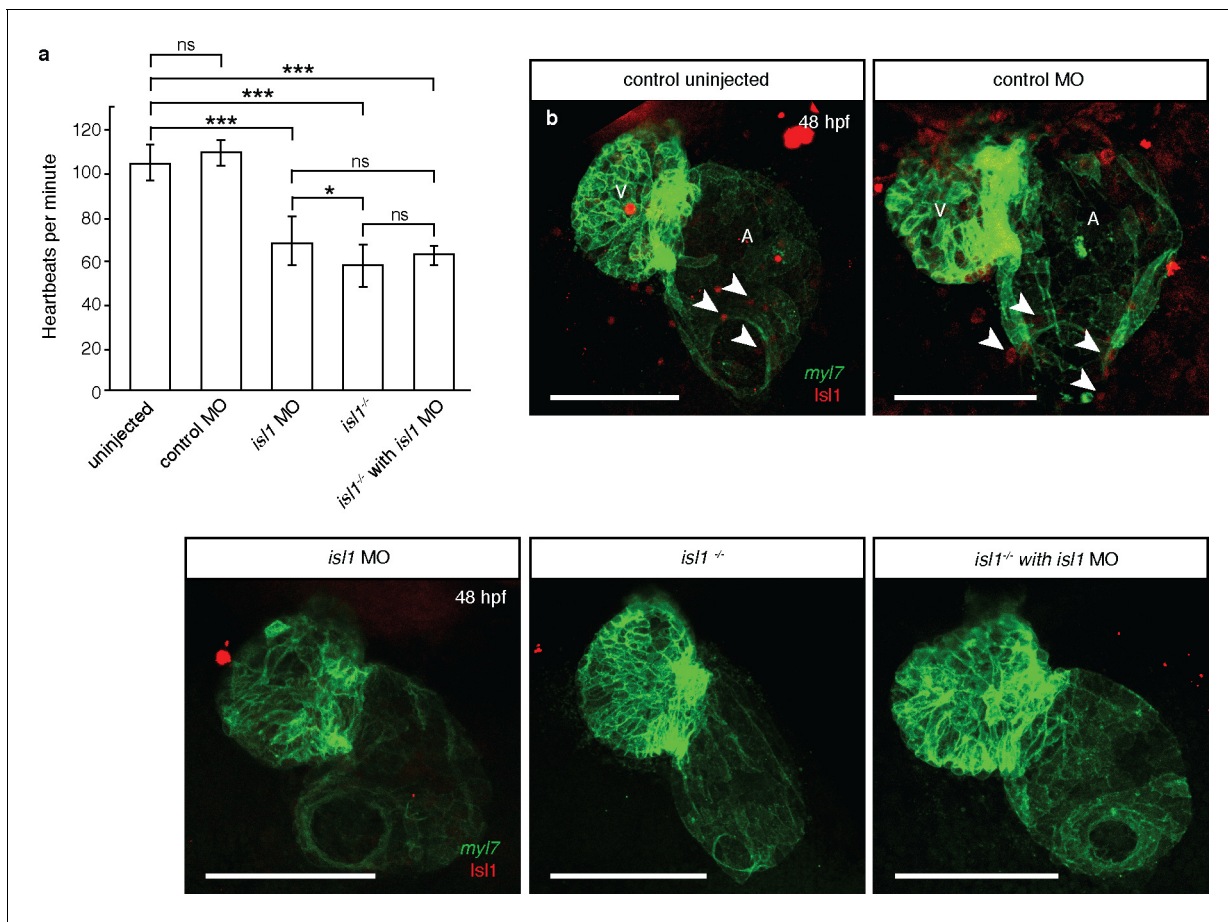


**Figure 5—figure supplement 1.** *isl1* morphants have reduced levels of Isl1 protein and phenocopy *isl1* mutants. (a) At 48 hpf, the heart rate of *isl1* morphants (n = 10) is significantly lower than that of uninjected (n = 13) or control morpholino injected (n = 12) embryos, and similar to that of *isl1* mutant embryos (n = 14), in agreement with previously published data (de Pater et al., 2009). The heart rate of *isl1* mutants that were injected with *isl1* morpholino (n = 3) do not show significant difference with that of *isl1* mutants or morphants. (b) Antibody staining for Isl1 in 48 hpf *Tg(myl7:HRAS-EGFP)* hearts (arrowheads) showing decreased levels of Isl1 protein in *isl1* morphants and mutants. Altogether, these data suggest that the observed cardiac phenotypes in *isl1* morphants are not caused by non-specific effects from the morpholino injections. Student t-tests were performed, \*p<0.05; \*\*p<0.005; \*\*\*p<0.0005; ns, not significant; error bars indicate  $\pm$ SD. Scale bars: 100  $\mu$ m.

DOI: <https://doi.org/10.7554/eLife.32833.020>

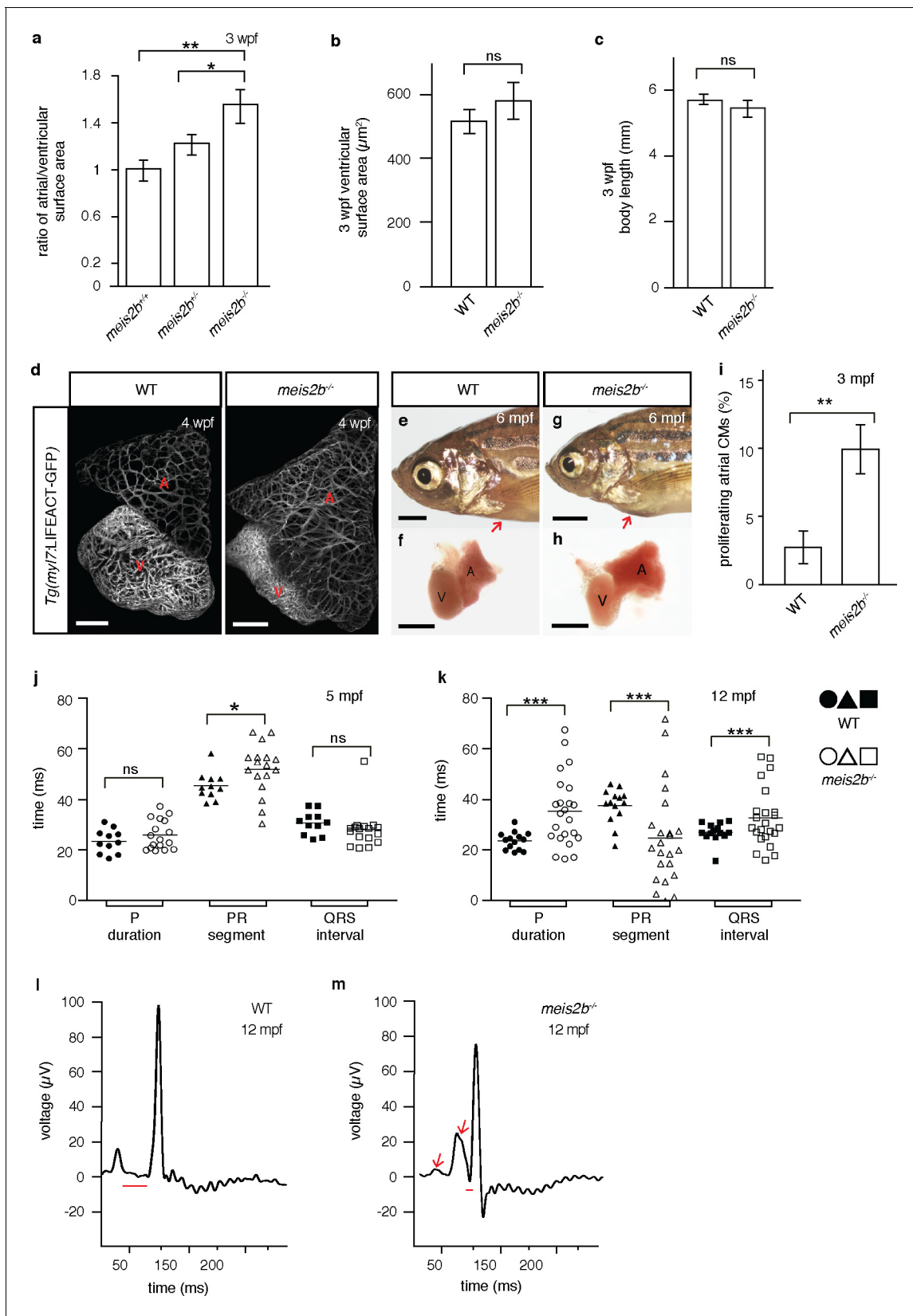


**Figure 6.** Loss of *meis2b* causes dysmorphic atrial growth and conduction defects. (a) *meis2b<sup>-/-</sup>* larvae exhibit a significant increase in the ratio of atrial to ventricular surface area, while (b) ventricular surface area and (c) body length are not affected compared to WT siblings. (d) Analysis of *Tg(myl7):LIFEACT-GFP*:

Figure 6 continued on next page



## Figure 6 continued

*LIFEACT-GFP* fish reveals no obvious defects in atrial myofibrillar architecture in 4 wpf *meis2b*<sup>-/-</sup>. (e–h) Adult *meis2b*<sup>-/-</sup> display pericardial bulging (arrow) due to abnormal atrial growth. (i) *meis2b*<sup>-/-</sup> exhibit a significant increase in atrial cardiomyocyte (CM) proliferation at 3 mpf. (j–k) Cardiac physiology assessed using electrocardiography (ECG) at 5 and 12 mpf. (j) *meis2b*<sup>-/-</sup> exhibit a significant increase in PR-segment variability compared to WT siblings, while P-duration and ventricular conduction (QRS) appear unaffected at 5 mpf. (k) At 12 mpf, PR-segment, P-duration and QRS interval are significantly affected in *meis2b*<sup>-/-</sup>. (l–m) Representative ECGs of 12 mpf animals show reduced PR-segment duration (red line) and multiple P-waves (arrow) in *meis2b*<sup>-/-</sup>. Scale bars: (d) 100  $\mu$ m, (e–h) 1 mm. (a–c, i) One-tailed student t-tests were performed. (j–k) F-test and Bartlett's test were performed. Significant differences compared with control are indicated (\* $p < 0.05$ ; \*\* $p < 0.005$ ; \*\*\* $p < 0.0005$ ); error bars indicate  $\pm$  SD. A, atrium; V, ventricle; ns, not significant.

DOI: <https://doi.org/10.7554/eLife.32833.025>

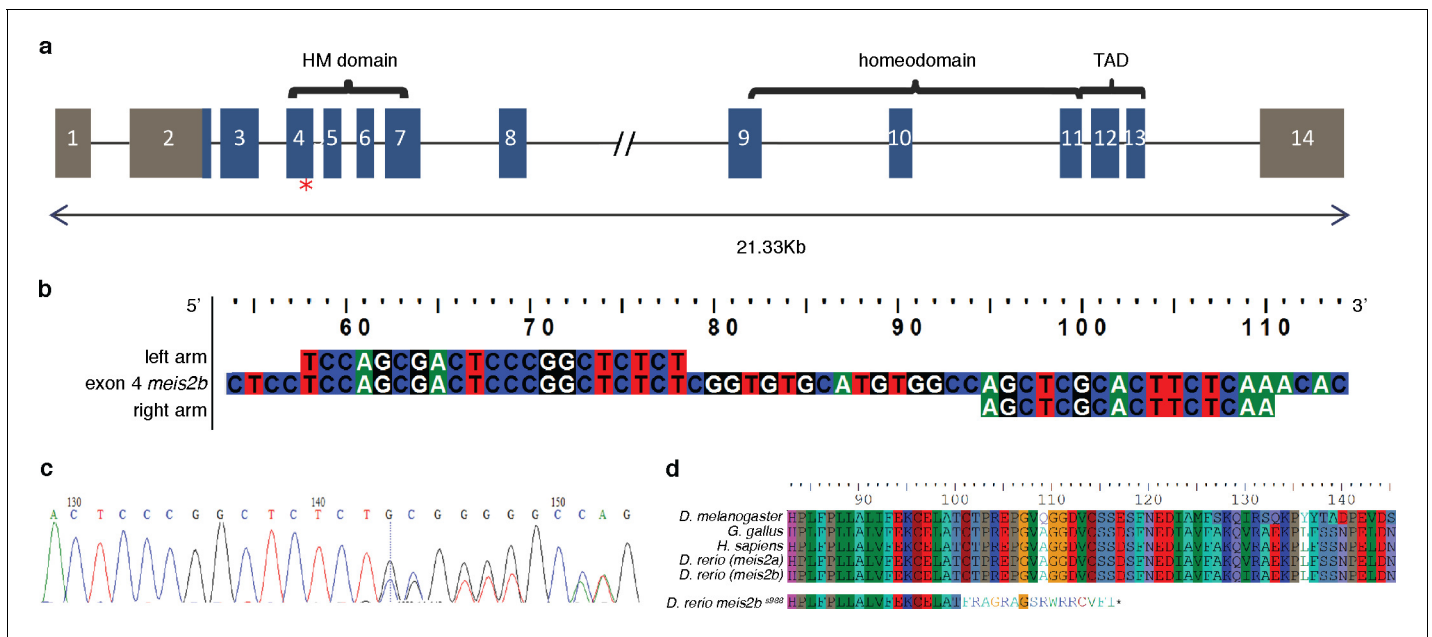


**Figure 6—figure supplement 1.** Generation of a *meis2b* mutant allele by TALEN mutagenesis. (a) Illustration of the genomic structure of *meis2b*. Exon 4 (red asterisk), which encodes part of the Hth/Meis (HM) domain, was targeted by site directed mutagenesis with a TAL effector nuclease (TALEN). (b) Sequence of the left and right TALEN arms. (c) Chromatogram showing the induced frameshift allele which carries a 10 base pair deletion and three base pair insertion. (d) Alignment of the translated coding sequence of the HM-domain of different species, illustrating the high level of conservation from arthropods to mammals at the site of the lesion. Translated *meis2b<sup>s988</sup>* coding sequence shows a premature stop 16 amino acids after the induced frameshift mutation. The resulting predicted protein lacks most functional domains, including the DNA-binding domain and the C-terminal transactivation domain (TAD).

DOI: <https://doi.org/10.7554/eLife.32833.026>

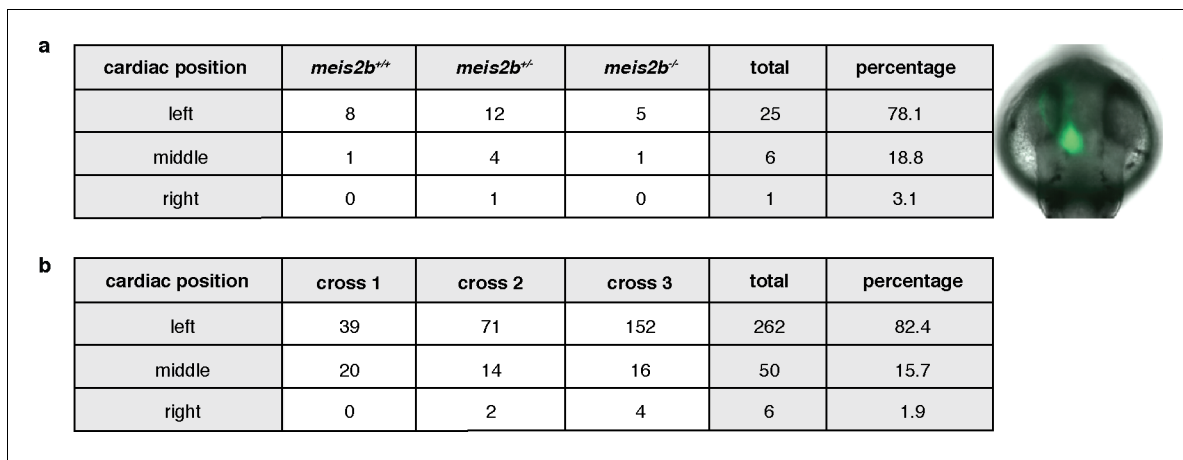


**Figure 6—figure supplement 2.** Cardiac positioning (jogging) appears unaffected in *meis2b* mutants. General body laterality is not affected in *meis2b<sup>−/−</sup>*. Cardiac jogging was assessed from the dorsal side (anterior to the top) using the *Tg(myl7:LIFEACT-GFP)* line, as shown in the picture on the right. (a) Cardiac jogging is not affected in *meis2b<sup>−/−</sup>*. (b) Assessment of cardiac jogging in three independent crosses of *Tg(myl7:LIFEACT-GFP)* WT fish.  
DOI: <https://doi.org/10.7554/eLife.32833.027>

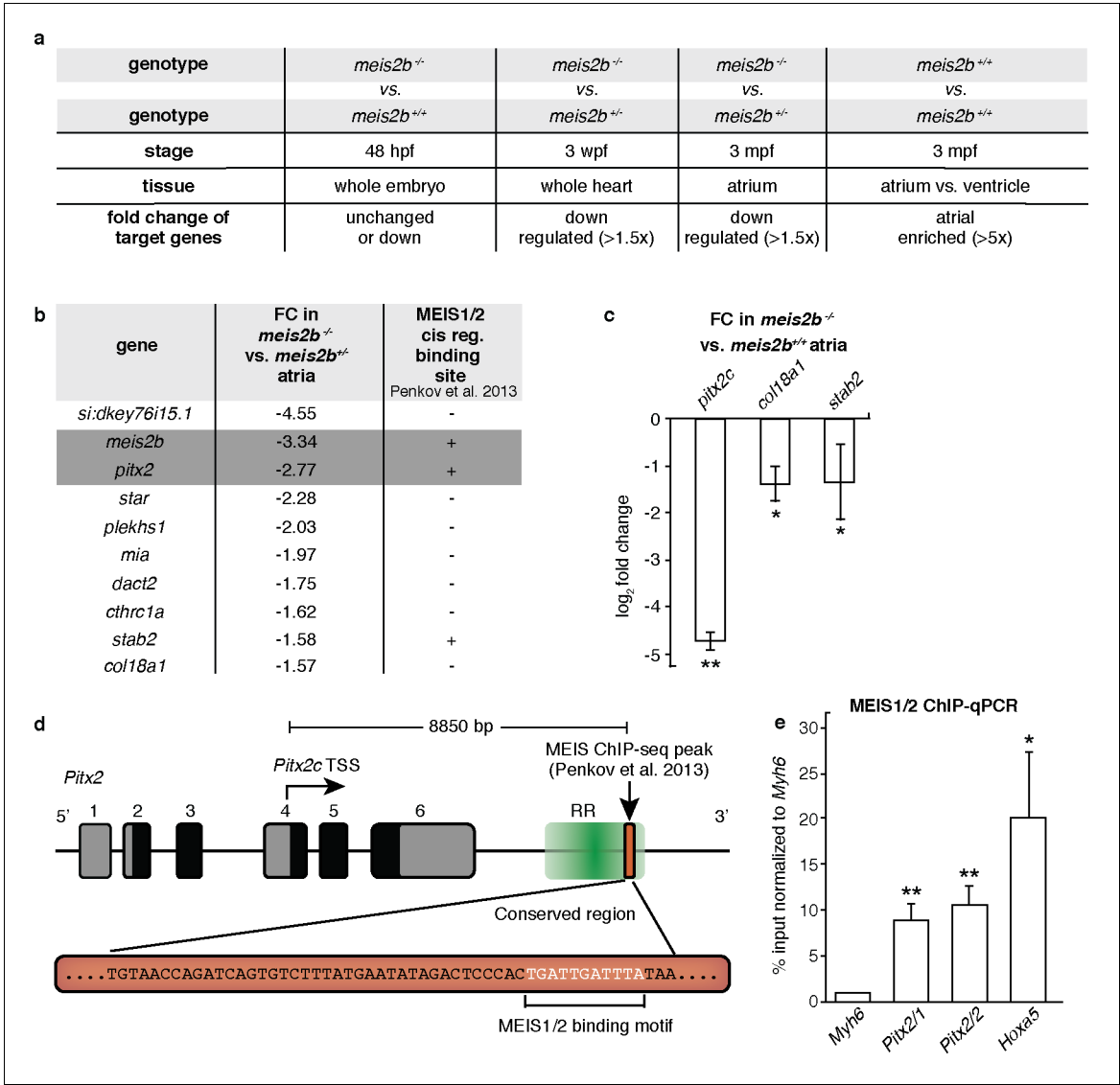


**Figure 7.** Meis2b positively regulates cardiac *pitx2c* expression. (a) Overview of the different samples used for microarray comparison, showing the stage, type of tissue and genotype of the compared samples. The bottom row shows the expected outcome of downstream genes potentially regulated by Meis2b. (b) Table showing the 10 genes fitting all selection criteria (for genes with  $n > 1$ , the values are averaged). Cis-regulatory MEIS1/2 DNA binding sites in orthologous mouse genes were extracted from (Penkov et al., 2013). (+, proximal binding site detected; -, no proximal binding site detected). (c) RT-qPCR analysis in *meis2b*<sup>-/-</sup> vs WT sibling atria. (d) Representation of the *Pitx2* locus in mouse indicating the location of a previously reported MEIS1/2 ChIP-seq peak at the 3' end of the regulatory region (RR) (ENSMUSR00000406450) (Penkov et al., 2013). A 53 bp conserved sequence inside the ChIP-seq peak is shown together with the MEIS1/2 binding motif. (e) ChIP-qPCR analysis on E12 embryonic mouse trunks of MEIS1/2 on the *Pitx2* locus shown in (d), on the *Hoxa5* locus (a known MEIS1/2 direct target), and on *Myh6* locus (used as a negative control). One-tailed student t-tests (c), and one-sample t-tests (e) were performed, significant differences compared with control are indicated (\* $p < 0.05$ ; \*\* $p < 0.005$ ); error bars indicate  $\pm$ SD.

DOI: <https://doi.org/10.7554/eLife.32833.029>

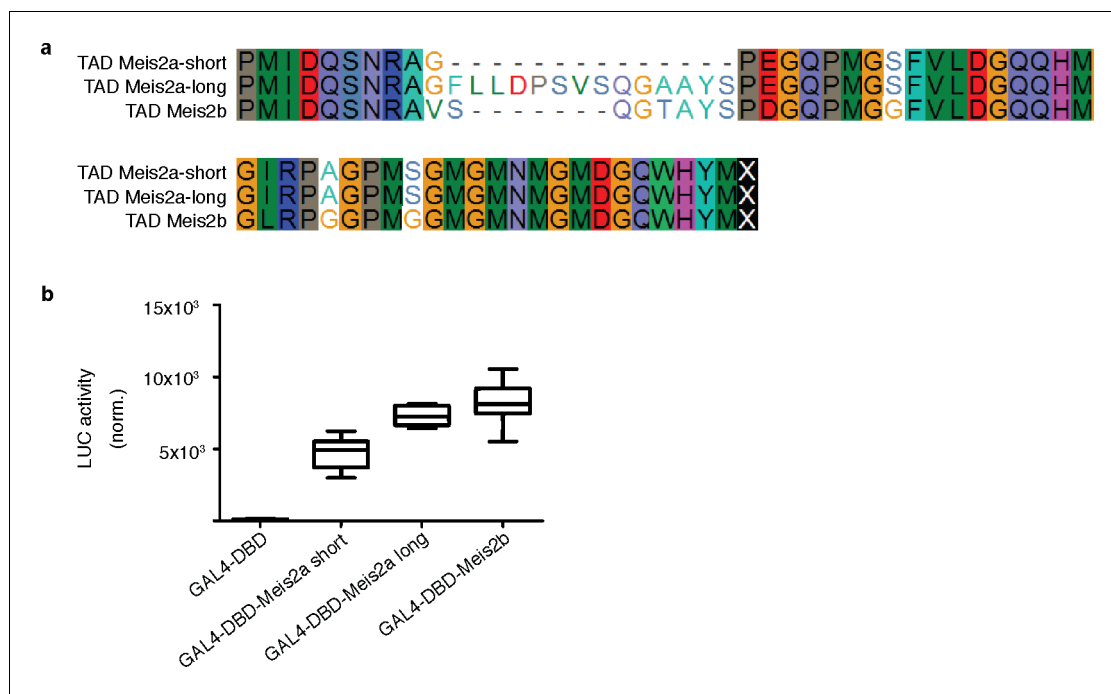


**Figure 7—figure supplement 1.** Transactivation potential of Meis2a/b C-terminal domains. The transactivation potential of cardiac Meis2 isoforms was investigated in vitro. (a) Alignment of the C-terminus of all Meis2a/b isoforms as detected by PCR in adult cardiac cDNA pools. (b) HEK293T cells were transiently co-transfected with plasmids encoding GAL4-DBD alone or GAL4-DBD fused to each of the Meis2 C-terminus shown in (a) together with an UAS:Luciferase reporter plasmid. Luciferase induction represents respective transactivation potential. Bar = median, box = 95% CI, whiskers = min/max, TAD = Transactivation domain. Error bars indicate  $\pm$ SD.

DOI: <https://doi.org/10.7554/eLife.32833.030>



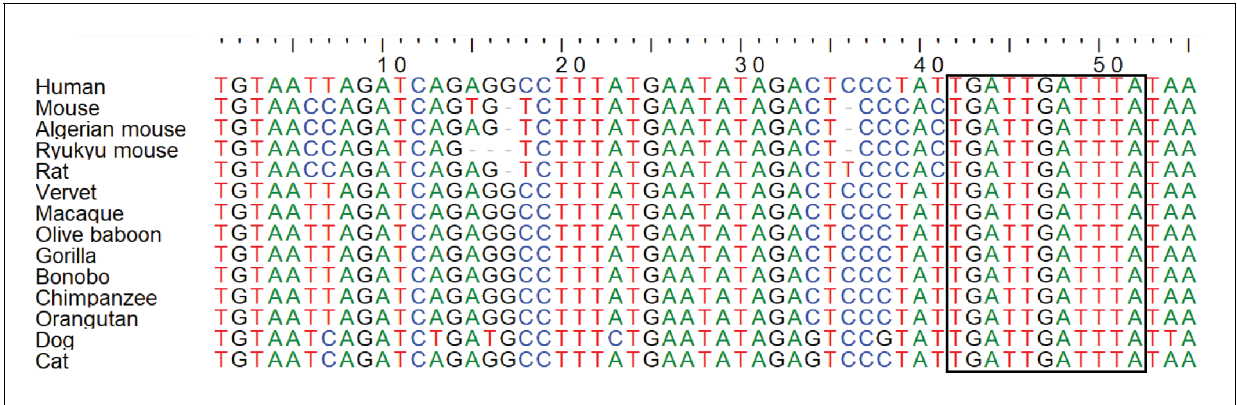


**Figure 7—figure supplement 2.** Conserved element inside ChIP-seq peak. The 53 bp long element found inside the MEIS1/2 ChIP-seq peak is highly conserved in many mammalian species and contains the MEIS1/2 binding motif (black square).  
DOI: <https://doi.org/10.7554/eLife.32833.031>